Heliyon 6 (2020) e03119

Contents lists available at ScienceDirect

Heliyon

journal homepage: www.cell.com/heliyon

Research article

Improved pyrolysis behavior of ammonium polyphosphate-melamine-expandable (APP-MEL-EG) intumescent fire retardant coating system using ceria and dolomite as additives for I-beam steel application

Joshua B. Zoleta [a,c,*], Gevelyn B. Itao [a], Vannie Joy T. Resabal [a], Arnold A. Lubguban [a], Ryan D. Corpuz [a], Mayumi Ito [b], Naoki Hiroyoshi [b], Carlito Baltazar Tabelin [c]

[a] Department of Materials and Resources Engineering and Technology, College of Engineering and Technology, Mindanao State University–Iligan Institute of Technology, Iligan City, 9200, Philippines
[b] Laboratory of Mineral Processing and Resources Recycling, Division of Sustainable Resources Engineering, Hokkaido University, Sapporo, 060-8628, Japan
[c] School of Minerals and Energy Resources Engineering, The University of New South Wales, Sydney, NSW, 2052, Australia

ARTICLE INFO

Keywords:
Chemical engineering
Materials chemistry
Materials science
Intumescent coating
Char formation
Ceria
I-beam
Thermal stability
Ammonium polyphosphate
Pyrolysis
Fire retardant
Dolomite
XPS

ABSTRACT

This study describes the effects of ceria (CeO_2) and dolomite [$CaMg(CO_3)_2$] additives on the pyrolysis behavior and fire resistive property of conventional intumescent flame retardant (IFR) coating system for I-beam steel substrate called ammonium polyphosphate-melamine-expandable graphite (APP-MEL-EG) system. The fire resistance of various formulations was evaluated using the standard vertical Bunsen burner fire test. Thermogravimetric analysis (TGA) was used to understand the degradation of coating formulations. Observations by scanning electron microscopy with energy dispersive X-ray spectroscopy (SEM-EDX) demonstrated that significant amounts of additives favored the formation of homogeneous compacted char structures, which were predominantly composed of carbon (C), phosphorus (P) and oxygen (O). These three main components of the char were also found to be in various binding combinations with other lighter elements like nitrogen (N) and hydrogen (H) as illustrated by the attenuated total reflectance Fourier transform infrared (ATR-FTIR) spectroscopy results. X-ray photoelectron spectroscopy (XPS) further suggest that polyethylene($[(CH_2–C_2H_2–CH_2)^{n-}]$) free radicals were abundant on the char surface for the two best formulations and the binding energy of this radical promoted the formation of aromatic carbon chains that enhanced the char's thermal stability. This means that the selection of appropriate additives and combinations of flame-retardant ingredients could significantly change the morphology of the char layer and improve its thermal stability during fire exposure.

1. Introduction

Technological advancements are the defining factors of industrialized countries along with the upgrade from cement-based to steel-based infrastructures. This innovation in construction also required an update on legislation and building safety regulations to ensure personnel and structural safety because steel loses its structural stability after prolonged exposure to temperatures exceeding 500 °C (e.g., fire incidents) (Camino et al., 1989; Feng et al., 2016; Gillani et al., 2016; Horacek and Pieh, 2000; Le Bras et al., 1998). To resolve this issue, researchers have developed intumescent coating—fire retardant materials—that protect and maintain the structural integrity of steel infrastructures during fire incidents (Feng et al., 2016; Wang et al., 2006; Xu et al., 2019; Yan et al., 2018). Figure 1 shows a schematic diagram of how conventional intumescent coatings are activated via pyrolysis to protect steel substrates. In the event of a fire, intumescent coatings swell and produce a char which serves as a protective barrier to suppress heat penetration and prolong the failure of steel substrates (Camino et al., 1989; Jimenez et al., 2006; Le Bras et al., 1998; Zoleta et al., 2019).

In recent years, researchers have used several additives to improve the fire-protective performance of intumescent coating for steel substrates. Feng et al. (2016), for example, used ceria (CeO_2) as a catalyst on an intumescent fire-retardant (IFR) system using polypropylene as the carbon source and found that the resulting coating produced an effective

* Corresponding author.
E-mail addresses: joshua.zoleta@g.msuiit.edu.ph, joshua_successor@yahoo.com (J.B. Zoleta).

https://doi.org/10.1016/j.heliyon.2019.e03119
Received 13 March 2019; Received in revised form 5 August 2019; Accepted 20 December 2019

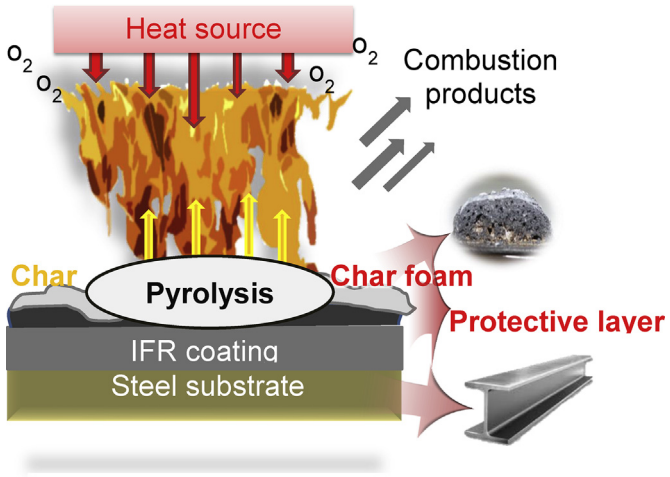

Figure 1. Pyrolysis mechanism of intumescent fire retardant coating.

char as early as 5 min after fire introduction but became unstable at temperatures higher than 250 °C. Similarly, Gillani et al. (2016) used dolomite [$CaMg(CO_3)_2$] as an additive on an IFR system using expandable graphite as the carbon source and showed that the resulting char had a more homogenous and compacted morphology that most likely stabilized char formation, which minimized the formation of holes and fractures that limited heat penetration.

In this study, a novel and more effective IFR coating using inorganic additives is proposed and its thermal protection performance on an I-beam steel substrate was evaluated. Ceria and dolomite were selected because the former is a known waste from glassmaking industries (Tabelin et al., 2013, 2018) while the latter is ubiquitous in limestone quarries (Eang et al., 2018a, b), sediments (Huyen et al., 2019a, b; Mar et al., 2013), waste rocks (Tabelin et al., 2012a, b; 2014, 2017a) and tailings of many gold mines (Aseniero et al., 2019; Opiso et al., 2018; Park et al., 2019). In addition to their beneficial use in the construction industry, finding value in these waste materials would also be good to the environment as a result of waste reduction for disposal from the glassmaking and mining industries.

2. Material and methods

2.1. Materials and reagents

Table 1 and Figure 2 summarize the formulations of different IFR samples and experimental design used in this study, respectively. The composition of each sample used in this study was optimized in the previous research of the authors (Zoleta et al., 2019). APP-EG-MEL IFR system consisting of ammonium polyphosphate (APP, average polymerization degree n > 1000, CAS No. 68333-79) as the acid source, expandable graphite (CAS No. 808067) as the carbon source and melamine (CAS No. 108-78-1) as the blowing agent were provided by Merteflor Enterprises while the fillers dolomite (99.99%, CAS No.16389-88-1) and ceria (CeO_2) (99.99%, CAS No. 1306-38-3) were purchased from Sigma Aldrich Singapore. The preparation of APP-EG-MEL (IFR system) with the addition of ceria and dolomite was based on the procedure of Gillani et al. (2016), which was modified and optimized in the previous research of the authors (Zoleta et al., 2019).

2.2. Fire protection test

The UL-94 vertical tests (bunsen burner fire test) were performed using a conventional methane-butane Bunsen with sample dimensions of 125 mm × 12.5 mm × 3.2 mm for 100 min. Thermocouples were attached at the back of the steel substrate and changes in temperature were recorded with time as discussed in the previous study of the authors.

2.3. Characterization and measurement

The morphology of char residues obtained after 100 min of fire exposure was examined by scanning electron microscopy with energy-dispersive X-ray spectroscopy (SEM-EDX) (Superscan SSX-550, Shimadzu Corporation, Japan). The machine was operated at an accelerating voltage of 15 kV, 1000x magnification and a working distance (WD) of 10 mm. The elemental maps were taken at 2,000 cps with 60 min time constant and high pixel resolutions of 256 × 256 (~60-minute scans).

A thermogravimetry-differential thermal analyzer (TG-DTA) (DTG-60H, Shimadzu Corporation, Japan) was used for the thermal gravimetric analysis (TGA) at a heating rate of 10 °C/min under air atmosphere with a flow rate of 40 ml/min using an alumina (Al_2O_3) crucible. Twelve milligrams (12 mg) of dried IFR coating samples were examined from 25 to 1000 °C according to ASTM E1131. All thermal degradation data was obtained from the TGA curves.

The char residue was also examined using an attenuated total reflectance Fourier transform infrared spectroscopy (ATR-FTIR) (FT/IR-6200 HFV and ATR Pro One attachment equipped with a diamond prism, Jasco Analytical Instruments, Japan). Fourier transform infrared (FTIR) spectroscopic techniques like ATR-FTIR and diffuse reflectance Fourier transform spectroscopy (DRIFTS) have been shown by many authors to be sensitive and reliable in identifying molecular coordination of ions and molecules in the structure of minerals (Jeon et al., 2020; Li et al., 2019a; Park et al., 2018a, b; Tabelin et al., 2017b, c) and organic molecules (Li et al., 2019b; Jeon et al., 2018). The permanent optical alignment was guaranteed by corner cube (retro-reflective) mirrors with auto-alignment for maximum energy. With a resolution of 0.7 cm^{-1} and an S/N greater than 25,000:1. The detector records the attenuated IR beam as an interferogram signal to generate an IR spectrum in the range

Table 1. Formulations of the different IFR coatings.

Sample I.D	IFR System (wt.%)				Additives (wt.%)			
					CeO_2	Dolomite	Epoxy	Hardener
Control	APP	EG	Boric Acid	MEL	0	0	44.00	22.00
Sample A	APP	EG	Boric Acid	MEL	1	0	43.33	21.67
Sample B	APP	EG	Boric Acid	MEL	0	1	43.33	21.67
Sample C	APP	EG	Boric Acid	MEL	1	1	42.67	21.33
Sample D	APP	EG	Boric Acid	MEL	2	1	42.00	21.00
Sample E	APP	EG	Boric Acid	MEL	1	2	42.00	21.00
Sample F	APP	EG	Boric Acid	MEL	2	2	41.33	20.67
Sample G	APP	EG	Boric Acid	MEL	3	3	40.00	20.00

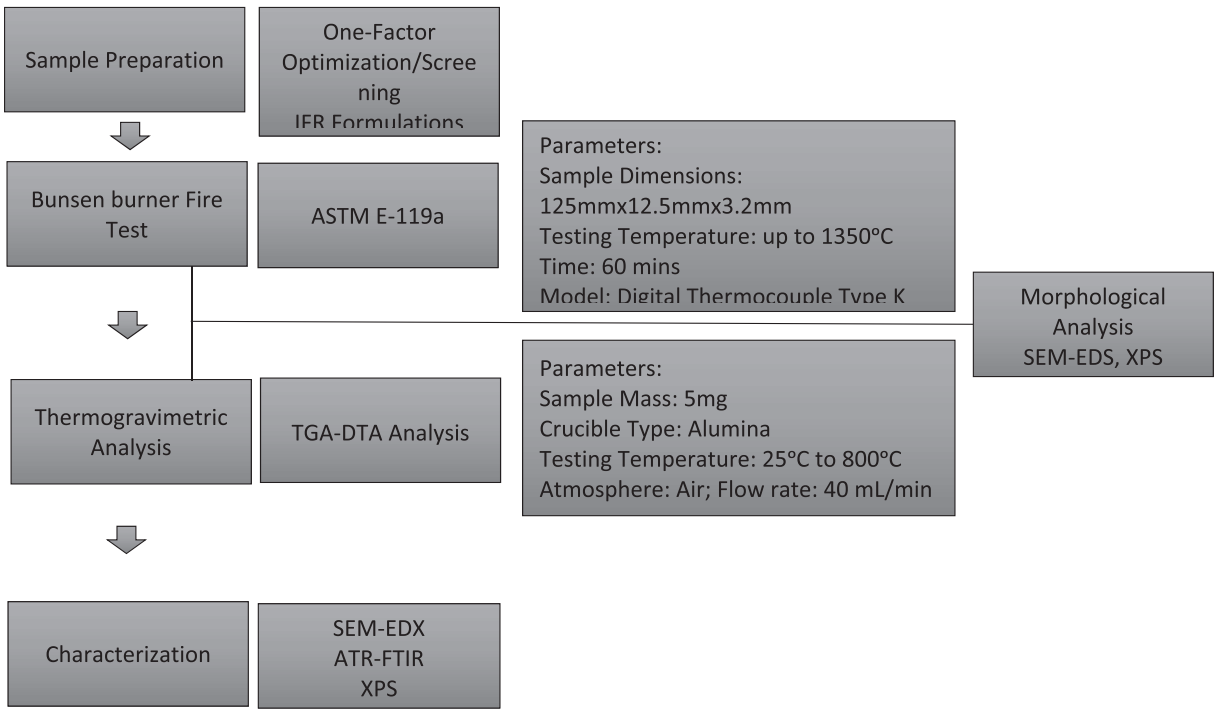

Figure 2. Schematic diagram of research design.

Table 2. Summary of thermogravimetric data of different IFR.

Sample I.D	Critical Temperature 1, CT1 (°C)	% Weight Loss (CT1)	% Weight Loss (Final)
Control	134.44	4.26	84.47
Sample C	130.80	5.69	81.79
Sample F	131.86	6.07	80.72

of 400–4000 cm^{-1}. The FTIR spectrum was deconvoluted by Gaussian fitting using Fityk software version 0.9.8 (Wojdyr, 2010).

X-ray photoelectron spectroscopic (XPS) analysis of the char residue was conducted using a JEOL JPS-9200 spectrometer (JEOL Ltd., Japan) equipped with a monochromatized Al Kα X-ray source operating at 100 W under ultrahigh vacuum (about 10^{-7} Pa). A narrow scan spectrum of oxygen ($O1_S$) and carbon ($C1_S$) were obtained and corrected using the binding energy of adventitious carbon (285.0 EV). All XPS spectra were deconvoluted with XPSPEAK version 4.1 using a true Shirley background and a 20–80% Lorentzian-Gaussian peak model (Shirley, 1972; Tabelin et al., 2019).

3. Results and discussion

Thermal properties of CeO_2-dolomite intumescent fire-retardant coatings. Table 2 summarizes the TGA data of the different IFR samples. It was observed that Samples C and F had the lowest percentage weight loss of about 82 and 81%, respectively compared with the 'Control' (i.e., sample without ceria and dolomite). Figure 3 shows the TGA curves of selected IFR coating formulations. The residual weight of the char decreased with the addition of inorganic additives at 100 °C. The

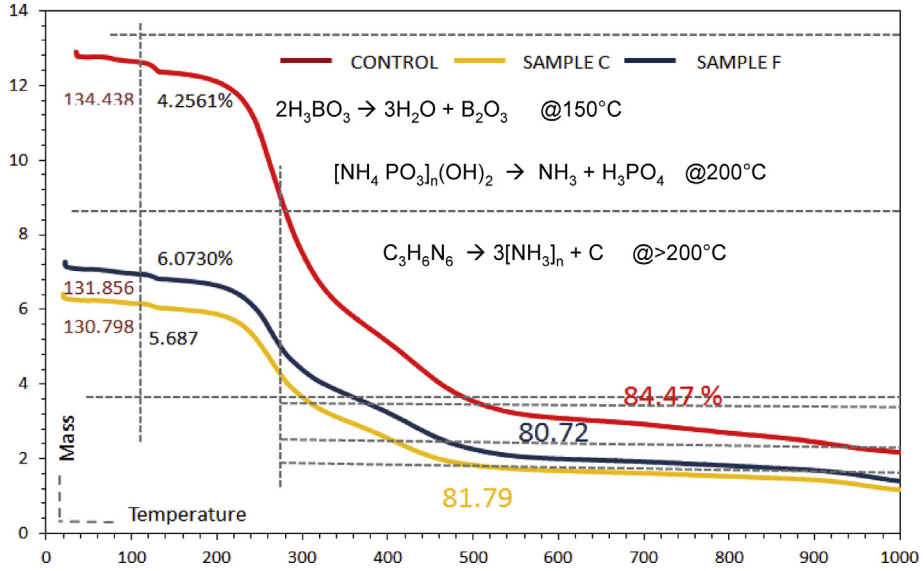

Figure 3. Detailed TGA graph of selected IFR formulation.

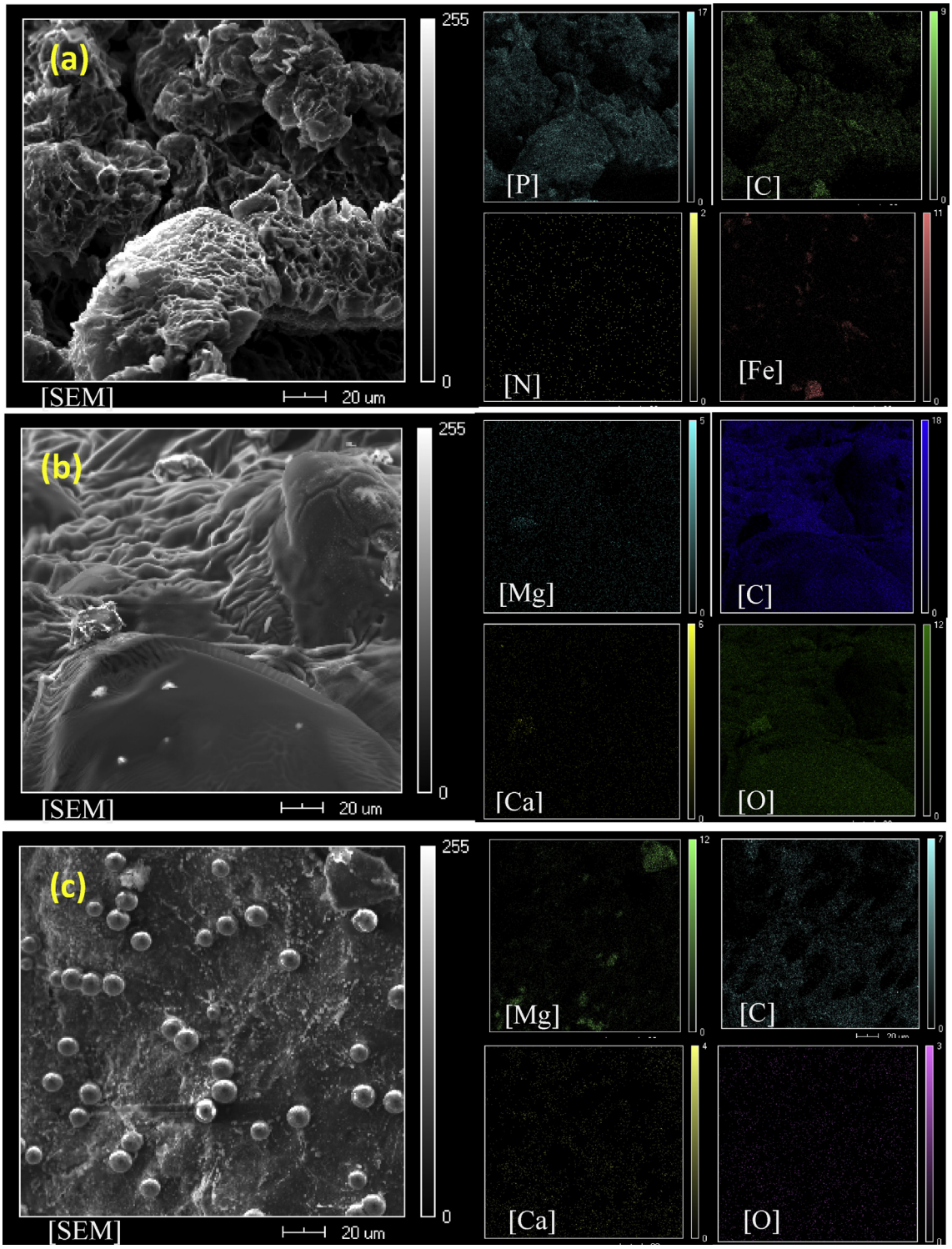

Figure 4. SEM photomicrographs of a.) Control b.) Sample C and c.) Sample F.

residual weight reduction in all ceria-dolomite IFR coatings was nominal below 150 °C, which could be attributed to the release of residual water primarily via dehydration of boric acid (Feng et al., 2016; Mohamad et al., 2013; Ullah and Ahmad, 2012). In the second stage between 200 and 300 °C, expandable graphite was degraded, resulting in about 25% loss of IFR coating mass. Around 250 °C, ammonium polyphosphate (APP) started to decompose and released ammonia (NH_3) gas, steam water (H_2O) and phosphoric acid (H_3PO_4) (Feng et al., 2016; Mohamad et al., 2013; Ullah and Ahmad, 2012). At this temperature, H_3PO_4 reacted with hydroxyl groups present in the IFR coating creating a network chain through dehydration. Melamine releases ammonia (NH_3) gas above 250 °C that expands the char framework making it more compact but spongy. It was observed that the addition of ceria and dolomite improved the expansion of char residues at higher temperatures.

It is important to note that fire resistance imparted the protective char layer mainly depends on its morphological structure. In order to define the roles of ceria and dolomite in the formation of char layer structure on intumescent phenomenon, residual chars of the different intumescent

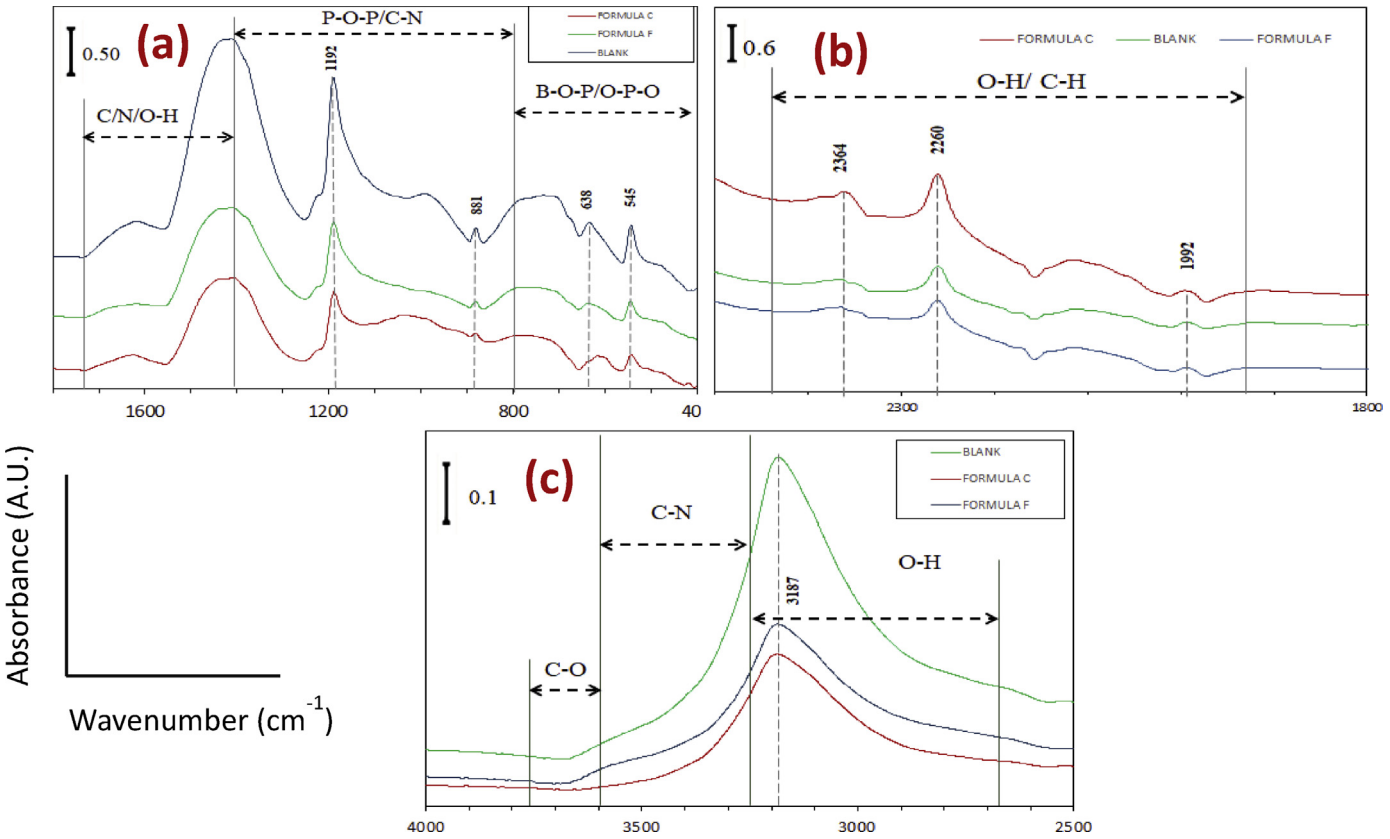

Figure 5. ATR-FTIR spectra of a.) Control, b.) Sample C, and c.) Sample F.

Table 3. Attribution of %Area of water (H_2O) obtained by ATR-FTIR from the different IFR samples.

Sample I.D	H_2O Area (1700–1400 cm^{-1})	H_2O Area (3700–3400 cm^{-1})
Control	31.76	187.60
Sample C	5.67	109.25
Sample F	7.13	110.56

Table 4. ATR-FTIR peak assignments for the different IFR formulations.

Wavelength, (cm^{-1})	Corresponding chemical structure	Reference
3700–3400	O–H in H_2O	Tabelin et al. (2017a, b, c)
3560–3546	C–O in CO_2, O–H in cyanic acid	Hoffendahl et al. (2014); Li et al. (2019a); Müller et al. (2016)
3090–3030	O–H in H_2O	
3016–2826	C–H in CH_4	
2354	C–O in CO_2, O–H in cyanic acid	
2284–2251	C–O in CO	
1820–1680	C=O, C=C	
1700–1400	O–H in H_2O	
1626–1603	N–H in NH_3, C–C, C=C, C–H	
1365	C–N	
1229–1216	O–H in cyanic acid	
1084	C–O in cyanic acid	
965–687	N–H in NH_3, C–C, C=C, C–H	

Table 5. Summary of % Area carbon from different binding energies.

Sample I.D	%Area of carbon		
	284.8 eV	286.1 eV	288.1 eV
Control	50.4365	27.8266	21.7369
Sample C	36.4994	32.1154	31.3851
Sample F	49.7321	28.4223	21.8455

coating formulations were characterized by SEM-EDX. Figure 4 displays the surface morphology of Control, Sample C and Sample F at 1000x magnification. Char of the Control (Figure 4a) did not exhibit any regular or homogeneous structure while those of Sample C and F had homogenous, continuous and dense char structures as illustrated in Figure 4b and c, respectively. It was observed that the outer surface of char from the Control had numerous holes and cracks, which could cause failure in heat shielding. In comparison, chars of Samples C and F had a more 'compact' and 'uniform' morphology with very little holes and cracks. It is also interesting to note that the additives, particularly dolomite, were detected on the char surface using SEM-EDX elemental mapping. This more compact and uniform char offered better protection that insulated the steel substrate from outside heat. The multiporous char layer could hinder heat transfer from the fire to the steel substrate and protect steel structures (Figure 4b and c). This means that a compact and solid char structure can increase the heat-insulating properties of IFR coating.

In order to understand the crosslinking of phosphorus (P) and oxygen (O) in the chars, ATR-FTIR was conducted. Figure 5 shows the ATR-FTIR spectra of the different IFR coating formulations. The IR spectra exhibited strong absorption peaks assigned to C–O, N–H, O–H, O–H, B–O–P, P–O–P and C–N crosslinking (Camino et al., 1978; Duquesne et al., 2013; Müller et al., 2016; Yew et al., 2015). Negligible crosslinking of C–O was

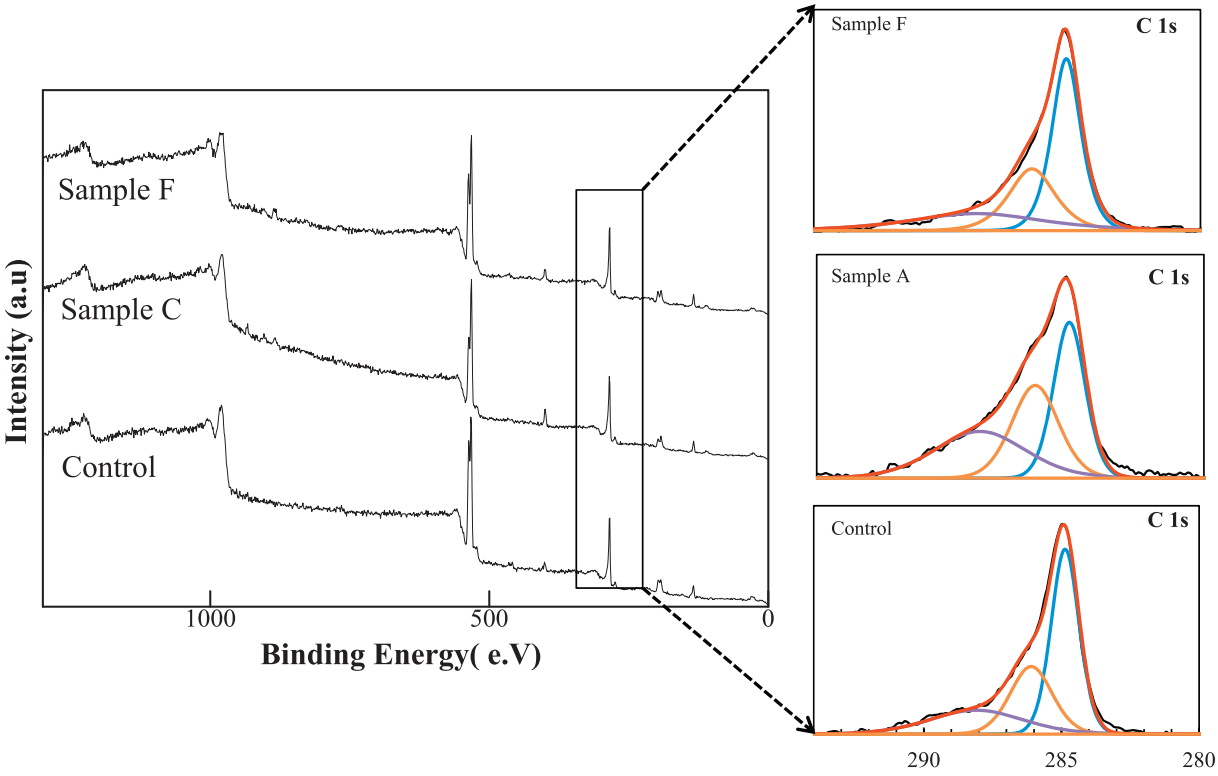

Figure 6. XPS narrow C_1s scan of selected IFR formulations.

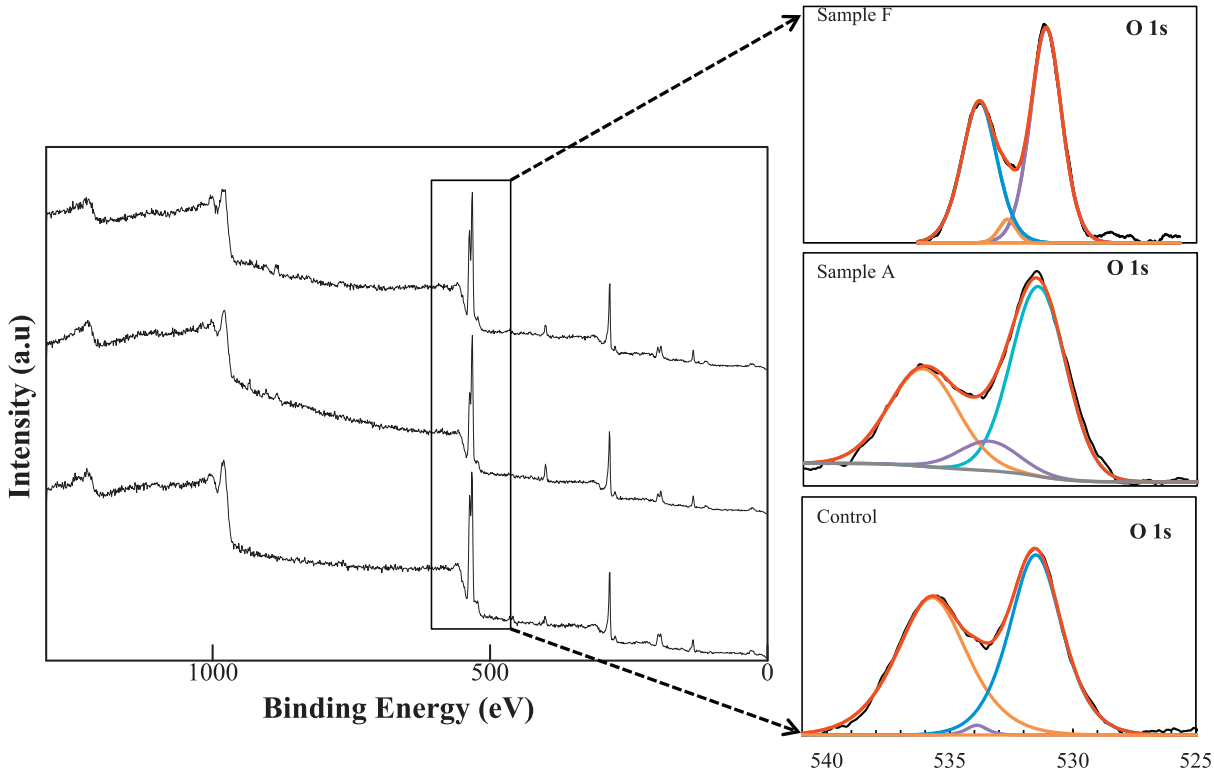

Figure 7. XPS Narrow O_1s scan of selected IFR Formulations.

Table 6. Summary of % Area oxygen (O_1s) from different binding energies.

Sample I.D	%Area of oxygen		
	531.5 eV	533.9 eV	535.7 eV
Control	49.0219	1.04764	35.1971
Sample C	55.4401	9.36276	49.9305
Sample F	55.5959	3.36234	41.0417

observed at wavelengths ranging from 3500 to 3800 cm^{-1} in all formulations as shown in Figure 5c. Moreover, all IFR samples have similar IR absorption patterns; that is, the characteristic absorption bands of the original polymer were detected (amine (N–H) at 1645 cm^{-1}, O–H at 3080 to 3300 cm^{-1}, C–H at 2850 to 2930 cm^{-1} and 1465 cm^{-1}). However, the strong intensities of O–H (3300–3300 cm^{-1}) attributed to water (H_2O) were undeniably noticeable in all formulations, such that, Tables 3 and 4 give its suggested abundance [11-15]. The relative abundance of water (H_2O) dramatically decreased after the addition of ceria, which suggests that it catalyzed and fastened the release of water from boric acid. This deduction is in good agreement with the TGA results, which showed that at around 130 °C, Samples C and F had lost more mass due to the release of water. Also, the release of water can be attributed to the favorable formation of more P–O radicals on the surface of the char, as it was relatively abundant in the SEM-EDS results shown in Figure 4 (see Table 5).

Surface characterization of the char layer from the IFR samples treated with standard vertical Bunsen burner fire test after 100 min was carried out by XPS and narrow scans for carbon (C_1s) and oxygen (O_1s) are presented in Figures 6 and 7, respectively. Figure 6 shows the deconvoluted C_1s peak of char layers of Control, Sample C and Sample F. The deconvoluted peak centered at 284.8 eV is assigned to —CH—CH— or C–C or C–O while at 286.1eV is attributed to C–O, C=O. Meanwhile, the deconvoluted peaks at 288.1 eV are related to the binding energies of C–O, C=C, C=O or C–C groups (Gillani et al., 2016). Compared with the Control, it is noted that more C–O from polyethylene structures were formed in Samples C and F, which indicates that more crosslinking structure containing C=O were formed, strengthening the barrier effect of char layer and suppressing further oxidation of the underlying materials (Gillani et al., 2016).

Figure 7 presents deconvoluted O_1s peaks of the char layers for the Control, Sample C and Sample F. The peak at 531.5 eV is assigned to single binding (O) in hydrogen or carbonyl groups, —CH—CH— or C–C or C–O [3, 16]. Also, the deconvoluted peak centered at 533.9 eV is attributed to O in C–C or C–O groups. Finally, the peak centered at 535.7 eV is assigned to O=O, C–O, C=O, and O–O of polyethylene (Gillani et al., 2016). As shown in Table 6, the chars formed by Samples C and F had more C–O species with binding energy at 533 eV. These results suggest that ceria incorporation into IFR promoted the formation of more crosslinking structures containing O, which agreed well with the C_1s XPS spectra. This ceria-catalyzed crosslinking reaction generated a substituted cyclohexane derivative of polyethylene, which was formed via organic chemical reactions between a conjugated '-diene' and a substituted alkene that agreed well with the ATR-FTIR results.

4. Conclusions

Thermogravimetric analysis (TGA) revealed that the addition of ceria and dolomite significantly improved the fire protection performance of IFR coating by increasing the quantity of residual weight left after thermal degradation. SEM-EDX photomicrographs also revealed the formation of a dense and compact char layer containing uniformly dispersed dolomite particles. It is proposed that dolomite improved the fire resistance of IFR coating due to its structural orientation and inherent refractory property. Furthermore, ATR-FTIR results suggest that ceria reinforced the strength of char during the fire test by not only catalyzing the release of water but also promoting the formation of P–O radicals. The study revealed that the ceria and dolomite addition to conventional APP-MEL-EG intumescent coating system significantly improved its thermal and fire-resistive properties during pyrolysis.

Declarations

Author contribution statement

Joshua Bravo Zoleta: Conceived and designed the experiments; Performed the experiments; Analyzed and interpreted the data; Wrote the paper.

Gevelyn Bontilao Itao, Carlito Baltazar Tabelin, Vannie Joy Resabal, Ryan Corpuz, ARNOLD LUBGUBAN, MAYUMI ITO, Naoki Hiroyoshi: Analyzed and interpreted the data; Contributed reagents, materials, analysis tools or data.

Funding statement

This work was supported by the Department of Science and Technology-Engineering Research for Development and Technology - A government funding agency in the Philippines. (amounting to 120,000 PhP).

Competing interest statement

The authors declare no conflict of interest.

Additional information

No additional information is available for this paper.

References

Aseniero, J.P.J., Opiso, E.M., Banda, M.H.T., Tabelin, C.B., 2019. Potential utilization of artisanal gold-mine tailings as geopolymeric source material: preliminary investigation. SN Appl. Sci. 1 (1), 35.

Camino, G., Costa, L., Martinasso, G., 1989. Intumescent fire-retardant systems. Polym. Degrad. Stab. 23 (4), 359–376.

Camino, G., Grassie, N., McNeill, I.C., 1978. Influence of the fire retardant, ammonium polyphosphate, on the thermal degradation of poly (methyl methacrylate). J. Polym. Sci. Polym. Chem. Ed. 16 (1), 95–106.

Duquesne, S., Bachelet, P., Bellayer, S., Bourbigot, S., Mertens, W., 2013. Influence of inorganic fillers on the fire protection of intumescent coatings. J. Fire Sci. 31 (3), 258–275.

Eang, K.E., Igarashi, T., Kondo, M., Nakatani, T., Tabelin, C.B., Fujinaga, R., 2018a. Groundwater monitoring of an open-pit limestone quarry: water-rock interaction and mixing estimation within the rock layers by geochemical and statistical analyses. Int. J. Mining Sci. Technol. 28 (6), 849–857.

Eang, K.E., Igarashi, T., Fujinaga, R., Kondo, M., Tabelin, C.B., 2018b. Groundwater monitoring of an open-pit limestone quarry: groundwater characteristics, evolution and their connections to rock slopes. Environ. Monit. Assess. 190 (4), 193.

Feng, C., Liang, M., Jiang, J., Huang, J., Liu, H., 2016. Synergism effect of CeO2 on the flame retardant performance of intumescent flame retardant polypropylene composites and its mechanism. J. Anal. Appl. Pyrolysis 122, 405–414.

Gillani, Q.F., Ahmad, F., Mutalib, M.I.A., Melor, P.S., Ullah, S., Arogundade, A., 2016. Effect of dolomite clay on thermal performance and char morphology of expandable graphite based intumescent fire retardant coatings. Proc. Eng. 148, 146–150.

Hoffendahl, C., Duquesne, S., Fontaine, G., Bourbigot, S., 2014. Decomposition mechanism of melamine borate in pyrolytic and thermo-oxidative conditions. Thermochim. Acta 590, 73–83.

Horacek, H., Pieh, S., 2000. The importance of intumescent systems for fire protection of plastic materials. Polym. Int. 49 (10), 1106–1114.

Huyen, D.T., Tabelin, C.B., Thuan, H.M., Dang, D.H., Truong, P.T., Vongphuthone, B., Kobayashi, M., Igarashi, T., 2019a. The solid-phase partitioning of arsenic in unconsolidated sediments of the Mekong Delta, Vietnam and its modes of release under various conditions. Chemosphere 233, 512–523.

Huyen, D.T., Tabelin, C.B., Thuan, H.M., Danga, D.H., Truong, P.T., Vongphuthone, B., Kobayashi, M., 2019b. Geological and Geochemical Characterizations of Sediments in Six Borehole Cores from the Arsenic-Contaminated Aquifer of the Mekong Delta, Vietnam. Data in Brief, 104230.

Jeon, S., Ito, M., Tabelin, C.B., Pongsumrankul, R., Kitajima, N., Park, I., Hiroyoshi, N., 2018. Gold recovery from shredder light fraction of E-waste recycling plant by flotation-ammonium thiosulfate leaching. Waste Manag. 77, 195–202.

Jeon, S., Tabelin, C.B., Takahashi, H., Park, I., Ito, M., Hiroyoshi, N., 2020. Enhanced cementation of gold via galvanic interactions using activated carbon and zero-valent aluminum: a novel approach to recover gold ions from ammonium thiosulfate medium. Hydrometallurgy 191, 105165.

Jimenez, M., Duquesne, S., Bourbigot, S., 2006. Intumescent fire protective coating: toward a better understanding of their mechanism of action. Thermochim. Acta 449 (1-2), 16–26.

Le Bras, M., Bourbigot, S., Camino, G., Delobel, R. (Eds.), 1998. Fire Retardancy of Polymers: the Use of Intumescence, 224. Elsevier.

Li, X., Hiroyoshi, N., Tabelin, C.B., Naruwa, K., Harada, C., Ito, M., 2019a. Suppressive effects of ferric-catecholate complexes on pyrite oxidation. Chemosphere 214, 70–78.

Li, X., Gao, M., Hiroyoshi, N., Tabelin, C.B., Taketsugu, T., Ito, M., 2019b. Suppression of pyrite oxidation by ferric-catecholate complexes: an electrochemical study. Miner. Eng. 138, 226–237.

Mar, K.K., Karnawati, D., Putra, D.P.E., Igarashi, T., Tabelin, C.B., 2013. Comparison of Arsenic adsorption on lignite, bentonite, shale, and iron sand from Indonesia. Proc. Earth Planetary Sci. 6, 242–250.

Mohamad, W.F., Ahmad, F., Ullah, S., 2013. Effect of inorganic fillers on thermal performance and char morphology of intumescent fire retardant coating. Asian J. Sci. Res. 6 (2), 263–271.

Müller, P., Morys, M., Sut, A., Jäger, C., Illerhaus, B., Schartel, B., 2016. Melamine poly (zinc phosphate) as flame retardant in epoxy resin: decomposition pathways, molecular mechanisms and morphology of fire residues. Polym. Degrad. Stab. 130, 307–319.

Opiso, E.M., Aseneiro, J.P.J., Banda, M.H.T., Tabelin, C.B., 2018. Solid-phase partitioning of mercury in artisanal gold mine tailings from selected key areas in Mindanao, Philippines, and its implications for mercury detoxification. Waste Manag. Res. 36 (3), 269–276.

Park, I., Tabelin, C.B., Seno, K., Jeon, S., Ito, M., Hiroyoshi, N., 2018a. Simultaneous suppression of acid mine drainage formation and arsenic release by Carrier-microencapsulation using aluminum-catecholate complexes. Chemosphere 205, 414–425.

Park, I., Tabelin, C.B., Magaribuchi, K., Seno, K., Ito, M., Hiroyoshi, N., 2018b. Suppression of the release of arsenic from arsenopyrite by carrier-microencapsulation using Ti-catechol complex. J. Hazard Mater. 344, 322–332.

Park, I., Tabelin, C.B., Jeon, S., Li, X., Seno, K., Ito, M., Hiroyoshi, N., 2019. A review of recent strategies for acid mine drainage prevention and mine tailings recycling. Chemosphere 219, 588–606.

Shirley, D.A., 1972. High-resolution X-ray photoemission spectrum of the valence bands of gold. Phys. Rev. B 5, 4709–4714.

Tabelin, C.B., Igarashi, T., Tamoto, S., Takahashi, R., 2012a. The roles of pyrite and calcite in the mobilization of arsenic and lead from hydrothermally altered rocks excavated in Hokkaido, Japan. J. Geochem. Explor. 119–120, 17–31.

Tabelin, C.B., Igarashi, T., Takahashi, R., 2012b. Mobilization and speciation of arsenic from hydrothermally altered rock in laboratory column experiments under ambient conditions. Appl. Geochem. 27, 326–342.

Tabelin, C.B., Igarashi, T., Yoneda, T., Tamamura, S., 2013. Utilization of natural and artificial adsorbents in the mitigation of arsenic leached from hydrothermally altered rock. Eng. Geol. 156, 58–67.

Tabelin, C.B., Hashimoto, A., Igarashi, T., Yoneda, T., 2014. Leaching of boron, arsenic and selenium from sedimentary rocks: I. Effects of contact time, mixing speed and liquid-to-solid ratio. Sci. Total Environ. 472, 620–629.

Tabelin, C.B., Sasaki, R., Igarashi, T., Park, I., Tamoto, S., Arima, T., Ito, M., Hiroyoshi, N., 2017a. Simultaneous leaching of arsenite, arsenate, selenite, and selenate, and their migration in tunnel-excavated sedimentary rocks: II. Kinetic and reactive transport modeling. Chemosphere 188, 444–454.

Tabelin, C.B., Veerawattananun, S., Ito, M., Hiroyoshi, N., Igarashi, T., 2017b. Pyrite oxidation in the presence of hematite and alumina: I. Batch leaching experiments and kinetic modeling calculations. Sci. Total Environ. 580, 687–689.

Tabelin, C.B., Sasaki, R., Igarashi, T., Park, I., Tamoto, S., Arima, T., Ito, M., Hiroyoshi, N., 2017c. Simultaneous leaching of arsenite, arsenate, selenite, and selenate, and their migration in tunnel-excavated sedimentary rocks: I. Column experiments under intermittent and unsaturated flow. Chemosphere 186, 558–569.

Tabelin, C.B., Igarashi, T., Villacorte-Tabelin, M., Park, I., Opiso, E.M., Ito, M., Hiroyoshi, N., 2018. Arsenic, selenium, boron, lead, cadmium, copper, and zinc in naturally contaminated rocks: a review of their sources, modes of enrichment, mechanisms of release, and mitigation strategies. Sci. Total Environ. 645, 1522–1553.

Tabelin, C.B., Corpuz, R.D., Igarashi, T., Villacorte-Tabelin, M., Ito, M., Hiroyoshi, N., 2019. Hematite-catalysed scorodite formation as a novel arsenic immobilisation strategy under ambient conditions. Chemosphere 233, 946–953.

Ullah, S., Ahmad, F., 2012. Enhancing the char resistant of expandable graphite based intumescent fire retardant coatings by using multi-wall carbon nano tubes for structural steel. In: Solid State Phenomena, 185. Trans Tech Publications, pp. 90–93.

Wang, Z., Han, E., Ke, W., 2006. Effect of nanoparticles on the improvement in fire-resistant and anti-ageing properties of flame-retardant coating. Surf. Coat. Technol. 200 (20-21), 5706–5716.

Wojdyr, M., 2010. Fityk: a general-purpose peak fitting program. J. Appl. Crystallogr. 43, 1126–1128.

Xu, Z., Chu, Z., Yan, L., Chen, H., Jia, H., Tang, W., 2019. Effect of chicken eggshell on the flame-retardant and smoke suppression properties of an epoxy-based traditional APP-PER-MEL system. Polym. Compos. 40 (7), 2712–2723.

Yan, L., Xu, Z., Wang, X., Deng, N., Chu, Z., 2018. Preparation of a novel mono-component intumescent flame retardant for enhancing the flame retardancy and smoke suppression properties of epoxy resin. J. Therm. Anal. Calorim. 134 (3), 1505–1519.

Yew, M.C., Sulong, N.R., Yew, M.K., Amalina, M.A., Johan, M.R., 2015. Influences of flame-retardant fillers on fire protection and mechanical properties of intumescent coatings. Prog. Org. Coat. 78, 59–66.

Zoleta, J., Itao, G., Resabal, V.J., Lubguban, A., Corpuz, R., Tabelin, C., Ito, M., Hiroyoshi, N., 2019. CeO_2-dolomite as fire retardant additives on the conventional intumescent coating in steel substrate for improved performance. In: MATEC Web of Conferences, 268. EDP Sciences, 04009.